Nanoscale

Accepted Manuscript

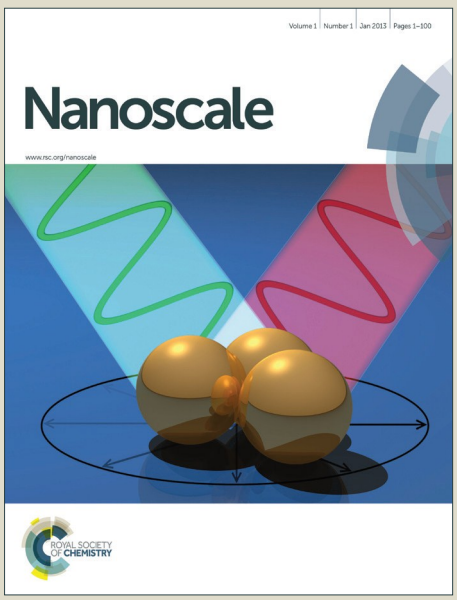

This is an *Accepted Manuscript*, which has been through the Royal Society of Chemistry peer review process and has been accepted for publication.

Accepted Manuscripts are published online shortly after acceptance, before technical editing, formatting and proof reading. Using this free service, authors can make their results available to the community, in citable form, before we publish the edited article. We will replace this *Accepted Manuscript* with the edited and formatted *Advance Article* as soon as it is available.

You can find more information about *Accepted Manuscripts* in the Information for Authors.

Please note that technical editing may introduce minor changes to the text and/or graphics, which may alter content. The journal's standard Terms & Conditions and the Ethical guidelines still apply. In no event shall the Royal Society of Chemistry be held responsible for any errors or omissions in this *Accepted Manuscript* or any consequences arising from the use of any information it contains.

ROYAL SOCIETY OF CHEMISTRY

www.rsc.org/nanoscale

Nanoscale

RSCPublishing

ARTICLE

Monocrystal Graphene Domain Biosensor array with differential output for Real-time Monitoring of Glucose and Normal saline

Cite this: DOI: 10.1039/xoxxoooooox

Junjie Shi,[a] Xin Li, [a] Qian Chen,[b] Kun Gao,[c] Hui Song, [a] Shixi Guo, [a] Quanfu Li,[a] Ming Fang, [a] Weihua Liu, [a] Hongzhong Liu [b] and Xiaoli Wang [ac]

Received ooth January 2015,
Accepted ooth January 2015

DOI: 10.1039/xoxxoooooox

www.rsc.org/

Biosensor array with differential output based on monocrystal graphene domain is proposed to realize high resolution measurement. The differential output structure can eliminate the noise that comes from graphene crystal orientation and grain boundary, as well as the fluctuation comes from the contact resistance and experiment process, so as to improve resolution in the lower concentration. We have fabricated high quality monocrystal graphene domain which has millimeter size via chemical vapor deposition method. Two identical graphene ribbons that are cut from the same domain are used as field effect transistor source-to-drain channels for reference and test of differential output, respectively. The experiment results show that source-to-drain current has a fast response shorter than 0.5 second in the glucose, normal saline and pH buffer solution of different concentrations. Sensitivity increases exponentially with the increase of concentration of tested liquid and high resolution range is 0.01~2 wt % in glucose and 0.0009~0.018wt % in saline, the highest resolution of glucose and saline are 0.01 wt % and 0.0009 wt %, respectively. We have fabricated 1×4 array structure with differential outputs that pave the way for rapidly detecting of ultralow concentration of analytes.

1. Introduction

[1]Graphene, a single layer of carbon atoms in a two-dimensional honeycomb lattice, has emerged as an attractive material due to its excellent electronic, chemical and physical properties since its discovery.[1-3] Electrical detection of biomolecules using graphene can achieve high sensitivity because the charge carries in graphene are restricted to an one-atom-thick plane, making graphene an consummate material for biological detection.[4-8]

In recent years, graphene biosensors have been researched by many groups. Most of graphene biosensor device is based on field effect transistor (FET) which is fundamental and important structure in silicon-based device fabrication. Yasuhide Ohno et al. demonstrated a label-free immunosensor based on an aptamer-modified graphene field effect transistor (G-FET). The aptamer-modified G-FET showed selective electrical detection of immunoglobulin E.[9] In the transfer characteristic of as-prepared graphene field effect transistors, Wangyang Fu et al. made a point that graphene channel is insensitive to pH value in solution, because it outputs Dirac point shifts when the pH value is changed.[10] Ying Wang et al. reported that graphene was successfully used in selective sensing of dopamine, they also indicated the prospective performances of graphene to other biological molecules including nucleic acids, proteins and enzymes.[11] And also Schedin et al. reported that graphene acquired by mechanical exfoliation could detect various gas molecules including NO_2, NH_3 and CO.[12] In above structure graphen channels are non-suspending. Cheng et al. reported enhanced performance of suspending grpahene field effect transisitors as sensors in aqueous. It has been found that trapped charges at the interface and in the oxide degrade transport characteristics of non-suspending graphene,[13-15]while graphene is suspending in solution, the device is advantageous to achieve low detection limit in solution.[16] The improved performance in suspending

1

[a] Department of microelectronics, School of Electronic and Information Engineering, Xi'an Jiaotong University, Xi'an,710049, China. E-mail: lx@mail.xjtu.edu.cn; Tel: +86-29 8266 3343.

[b] State Key Laboratory for Manufacturing Systems Engineering, Xi'an Jiaotong University, Xi'an 710049, China.

[c] School of Life Science and Technology, Xi'an Jiaotong University, Xi'an 710049, China

Nanoscale Accepted Manuscript

graphene shows that device degradation associated with charges at the interface is superior to non-suspended devices. However, the graphene is unable to avoid being affected by contact trouble. The above graphene devices are based on single output structure that graphene is highly affected by the contact resistance.

The contact between graphene and electrodes is comparably important to the sensitivity of device. At this stage, the role of the metal-to-graphene contact is at the forefront of obstacles which impede the further improvement in performance.[17-21] Joshua T. Smith et al. consider that the performance of graphene electronics is limited by contact resistance associated with the metal-graphene interface where transport characteristic degrades as carriers are injected from a 3-dimension metal to a 2-dimension graphene sheet.[22] Carrier transport can be envisaged as two cascading events including injection from metal to the graphene sheet and the following transport into the channel region.[23] Although the contact resistance(<1KΩ) has been studied and obviously improved, it is still not enough for practical application. Device structure of innovation should be paid more attention to improve the performance.

On the other hand, the quality and size of graphene has a significant effect on sensitivity of sensor, so the preparation of graphene has always been the focus of frontier research. [24-26] Grphene can be made by mechanical exfoliation or chemical vapor deposition (CVD),[27-30] and can be easily transferred to rigid or flexible substrate for integration. At low pressure, the growth of graphene on copper copper foil by chemical vapor deposition (CVD) method is a self-limiting process, that is to say, the growth process stops after a single graphene layer forms.[31-32] Single layer graphene is always polycrystalline structure that consists of many monocrystal domain, as well as different graphene crystal orientation and a lot of grain boundary that caused carrier transport noise. As we said before, the above device structures have only single output that graphene source-to-drain channel is sensitive to surrounding influence such as contact resistance difference, crystal orientation and grain boundary.

We propose a differential output structure with a pair of identical graphene ribbons cut from the same monocrystal domain that can confirm the identical crystal orientation and eliminate the influence of grain boundary, so as to eliminate the influence of noise which comes from graphene crystal orientation difference, grain boundary, contact difference and test process. Graphene used in our paper is grown by chemical vapor deposition(CVD) method because we can acquire the millimeter size of monocrystal graphene domain which is big enough to cover the whole biosensor array of 1×4. The e-beam lithography, rapid thermal annealing and oxygen plasma are used in our experiment to improve the ohmic contact. In this paper, the objects to be tested include Glucose, normal saline and pH buffer solution, the concentration of those is important indicator in medicine field.

2. Experimental details

The structure of proposed differential output biosensor array based on monocrystal graphene domain is shown in FIGURE 1a. Two identical graphene ribbons come from the same graphene domain are used as source-to-drain channels. The electrodes of source and drain are deposited on garphene ribbon. The micro liquid channel made up of SU-8 wall is placed upon the electrodes, and used for separating test liquid from testing probes in order to avoid short current between source and drain. The substrate consists of silicon dioxide (300nm) insulator and N+ heavy doped silicon back gate.

The overall process for fabrication of the proposed graphene sensors on silicon dioxide is depicted in Fig. 1b. Graphene domains were grown on copper foils by the CVD method with a mixture of methane (0.2 sccm) and H_2 (100sccm) gases at 1077℃ for one hour and spin-coating with PMMA (poly methlmethacrylate), which has been reported in our previous work.[26] The size of graphene copper was about 10mm×10mm. Then the copper foil was etched in 5 wt % solution of ammonium persulfate ($(NH_4)_2S_2O_8$) for 1-2 hours, followed by cleaning in deionized water for several minutes which was shown in step (1') to (3'). There are four masks were used in our experiment for fabricating alignment mark, graphene ribbon channel, electrode array and SU-8 channel. And we have designed alignment marks to confirm the precision of alignment for multi layers lithography. Firstly, to verify the coordinate of the graphene domain, the alignment mark (mask-I) made of aluminum is prepared by the e-beam lithography (Cello Technology, Ohmiker-50BR) as shown in step (2). Then the graphene-PMMA structure was transferred onto the substrate, after that, the PMMA was removed by acetone in step (3). To achieve differential output, a pair of identical graphene ribbon was obtained by oxygen plasma (CETC 13 and Heibei Shentong Photoelectric technology Co. LTD, DQ-500C) etching process (mask-II) in step (4). Then source-to-drain electrode array was manufactured by the e-beam lithography again to realize the contact resistance (mask-III). After the e-beam lithography, the electrodes were treated by rapid thermal annealing (Allwin 21 Corp. RTA Heatpulse 410) to improve the contact between graphene and electrodes in step (5). Finally, the SU-8 photoresist was used to make the wall of micro liquid channel (mask-IV) for liquid testing.

A semiconductor parameter analyzer (Keithley Instruments, Inc., 4200 SCS) was utilized to monitor the source-to-drain current I_{DS} of each differential output during the test. Various concentrations of liquid solution including glucose, normal saline and acid-base liquor pH buffer were introduced to the micro liquid channel and then the (DI) water was introduced to clean the channel for recovery process. The monocrystal graphene morphology is investigated by scanning electron microscopy (SEM) (S-4800 field emission scanning electron microscope) and optical microscope (Olympus Corp., BX 51). Raman spectra were collected by Horiba Jobin Yvon HR 800 using a 514 nm laser excitation.

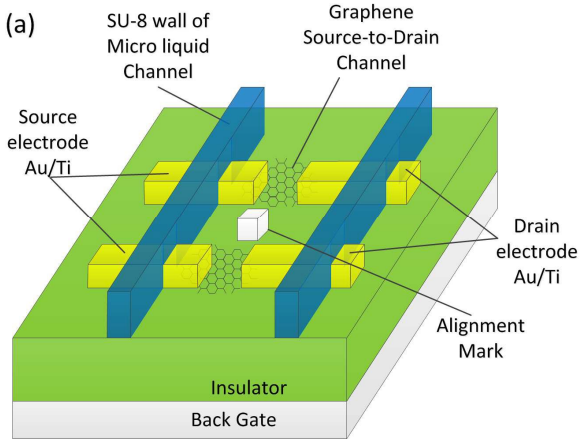

Nanoscale Accepted Manuscript

This journal is © The Royal Society of Chemistry 2012

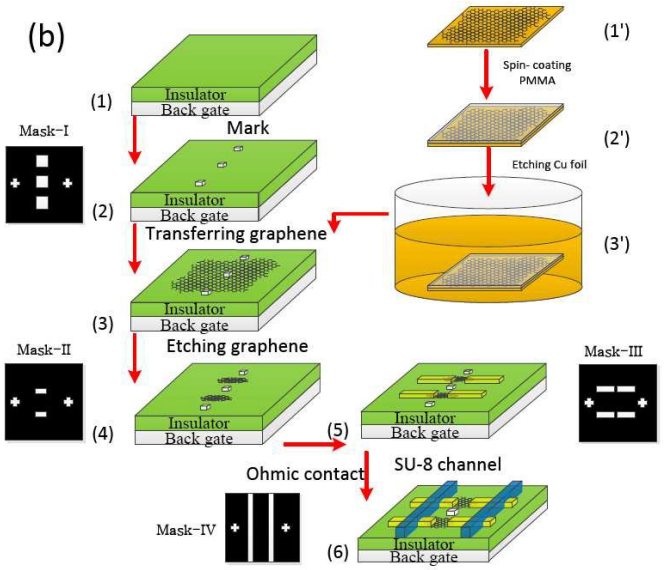

FIGURE 1: Schematic diagram(a) and fabrication flowchart(b) of the single layer monocrystal graphene domain biosensor array with differential output. In Figure (a), the graphene ribbons formed by oxygen plasma were underneath the electrodes composed of Au(100nm) and Ti(50nm) metal. The micro liquid channel is upon both graphene ribbons the electrodes by SU8 walls and for liquid solution test. In Figure (b), step (2) shows the preparation of alignment mark which is the coordinate markers for the following process steps. Step (1'), (2'), (3') and (3) depict the process of transferring graphene to substrate. Step (4) describes the oxygen plasma etching process to achieve a pair graphene ribbon of the differential structure. Step (5) shows source and drain electrode array was manufactured by e-beam lithography. Finally, the micro liquid channels made of SU-8 photoresist were produced by lithography process in step (6).

3. Results and Discussion

3.1 Morphology of Graphene and the Device Structure

The graphene used in our experiment is discrete film composed of high density ordered hexagonal monocrystal graphene domain as shown in Figure 2 (a), in which the size is nearly 1 millimeter. The G band and the 2D band have peaks at around 1583 CM^{-1} and 2664 CM^{-1}, respectively. The I_{2D}/I_G ratio is about 4.7 (Figure 2 (a) inset). These results confirmed that the graphene we used is monocrystal and single layer without defect peak. One monocrystal graphene domain is big enough for cover more than three ribbons that are orange rectangular patterns as shown in upper half of Figure 2 (b). The millimeter size of graphene domain is indispensable to realize the differential output. After etching process, pairs of graphene ribbons that are green rectangular patterns were left as shown in lower half of Figure 2 (b). The intact device structure which has the differential output of 1×4 is show in Figure 2 (c), the scale bar is 300 micrometers and the size of the array structure is about 600 micrometers. The size of one graphene ribbon is 30 × 100 micron square. The SU-8 walls stand still on top of electrodes and bent into a closed cavity for liquid solution test, as shown in lower left corner of Figure 2 (d). The 1×4 arrayed structure with differential outputs contains two 1×2 arrayed structure, and could detect two kinds of tested solution as glucose and normal saline. The 1 × 2 arrayed structure is composed of two identical graphene ribbons stemming from the same monocrystal graphene domain so that the ribbons have duplicate crystal orientation.

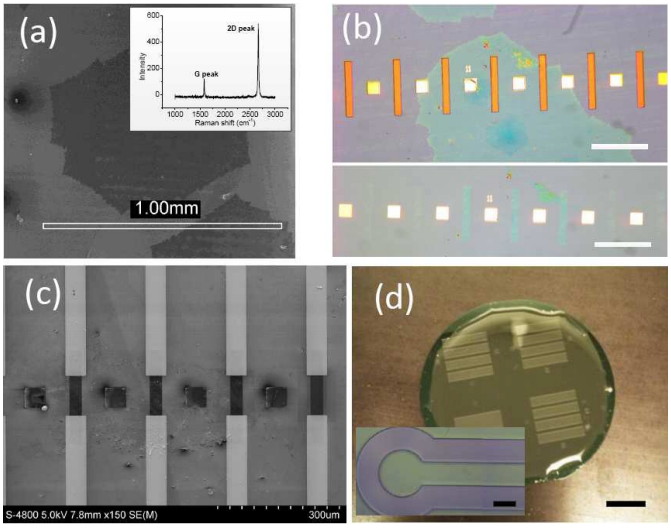

FIGURE 2: Microphoto of graphene morphology and device structure. (a) SEM image of graphene on Cu foil and Raman spectra of graphene transferred onto SiO_2/Si substrate. The G band and 2D band are peaked at around 1583 CM^{-1} and 2664 CM^{-1}, respectively. The scale bar is 1 millimeter. (b) Optical image of graphene ribbons from one monocrystal domain before (upper half) and after (lower half) etching process. Pairs of graphene ribbon was obtained by oxygen plasma (scale bar 100 microns). (c) SEM image of biosensor array with differential output, white rectangular patterns are electrodes and black ones are graphene. The size of array structure is about 600 micrometers (scale bar 300 microns). (d) Digital photos of device package and SU-8 wall for liquid channel. The height of SU-8 is about 465 microns(scale bar 10 mm, inset scale bar 30 microns).

3.2 pH Value Measurement in Single Output

Before the differential output structure test, we investigate study single output one. When the pH buffer solution flows into a single output micro liquid channel, the solution ions would be absorbed to the surface of the monocrystal graphene ribbon to change the transport characteristic. The source-to-drain current I_{DS} is modulated by the adsorbed ions as shown in Figure 3 (a). The I_{DS} changes immediately when the pH buffer is introduced into the micro liquid channel (in Figure 2d), the response times of three curves are all less than 0.5 seconds. We find that the device has a similar response both in acidic solution of pH 4.00 and alkaline solution of pH 9.18, respectively. Relative sensitivity, which is defined as $S = (I_{DS\,(INI)} - I_{DS\,(RES)}) / I_{DS\,(INI)}$, is used to measure the degree of device response caused by the change of pH value. $I_{DS(INI)}$ is initial steady current, $I_{DS(RES)}$ is steady response current, I_{DS} change is $I_{DS\,(INI)} - I_{DS\,(RES)}$. S in both of acidic and alkaline solution is higher than 50% and S in DI water neutral solution is lower than 30% as shown in Table 1. Because the ion concentration in both acidic and alkaline solution is higher than that in DI water, that have more significant influence on the conductivity of graphene. To distinguish pH buffer solution acidic or alkaline, we can observe the Dirac point shift D_{shift} in Figure 3 (b) and Table 1. The point in minimum conductivity is

Nanoscale Accepted Manuscript

called Dirac point, where carriers change from hole to electrons. In neutral DI water which pH was 6.86, we find the Dirac point is about 0V. It means that graphene keep intact and non-doping in ambient solution. Dirac point shifts toward more negative gate voltages with increasing pH values as shown in Figure 2 (b). There are two mechanisms in this process including surface charge effect and doping effect.[31] Surface charge effect means that ions move according to their charged polarity and accumulate to form electric layer at the interface between graphene and solution acting as a gate capacitor. As a result of negative charged hydroxyl groups (as Alkaline) attached to the graphene ribbon, the increased hole concentration leads to the Dirac point shifting to positive voltage and enhancing current I_{DS} with increasing pH value. On the contrary, Doping effect means that ions in solution dope the graphene from ribbon edge, and cause redundant defects and dangling bonds. Subsequently, carrier transport in graphene decreased, as well as current I_{DS} and conductivity. As a result of doping effect, the increased electron concentration leads to the Dirac point shifts to negative voltage with increasing pH value. Under the two kinds of effect, the Dirac point shifts to negative voltage with increasing pH value due to stronger doping effect.

In our graphene ribbons differential output structure experiment, current I_{DS} decreased instead of increased, because the doping effect plays a dominant role in the changing of conductivity instead of surface charge effect which is more common to graphene obtained by exfoliation method.[32] It is worth to note that the device could keep similar initial value, even after acidic and alkaline liquid experiment. However, there is some fluctuation in red line and blue line before black "liquid in"arrow (as shown in Figure 3a) when test liquid solution is introduced in SU-8 wall micro liquid channel. Noise introduced by experiment process and external environment is hard to avoid in single output structure, but is easy to eliminate in differential output structure.

Table 1 List of I_{DS} change, Sensitivity and Dirac point shifts towards pH value of single output structure testing

species	Acidic	DI water	Alkaline
pH	4.00	6.86	9.18
I_{DS} change	8.78 μA	4.57μA	9.62μA
S	54.17%	28.35%	58.04%
D_{shift}	0.33V	0V	-0.19V

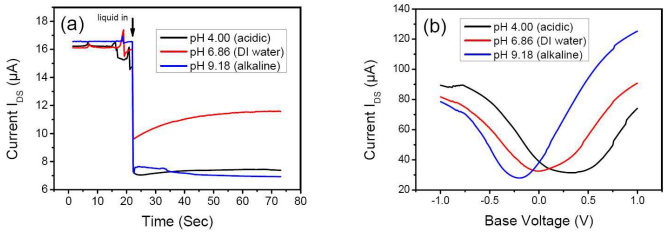

FIGURE 3 Source-to-drain current profile of different pH value solution. (a) I_{DS} versus time response and (b) I_{DS} versus base voltage response under DI water (red line), acidic (black line) and alkaline (blue line) solution. Dirac point shifts from positive to negative voltage with the increasing pH value from 4.00 to 9.18. Base voltage is applied in liquid from -0.1V to +0.1V.

3.3 Glucose and Normal saline Measurement in Differential Output

The concentration of glucose and normal saline are important indicator in medicine science. The real-time monitoring of glucose and saline is extremely significant to human health. In differential output structure, DI water is used to be reference, which is introduced in reference micro liquid channel, because it has the same pH value as glucose and normal saline solution, which are respectively introduced into testing micro liquid channel. The Source-to-drain current profile of glucose is shown in Figure 4. To explore the highest resolution of monocrystal graphene ribbon biosensor, we prepared six kinds of concentration by diluting standard glucose solution with DI water 5, 10, 50, 100 and 1000 times, respectively. Differential I_{DS} is defined as $\Delta I_{DS} = I_{DS\,(e.\,g.\,\%)} - I_{DS\,(DI\ water)}$, and Relative sensitivity is defined as $S = (I_{DS\,(e.\,g.\,\%)} - I_{DS\,(DI\ water)}) / I_{DS\,(e.\,g.\,\%)}$ that shows contrast at each concentration of glucose are shown in Table 2 and Figure 4 (b). Where $I_{DS\,(DI\ water)}$ and $I_{DS\,(e.\,g.\,\%)}$ are Source-to-drain current in reference and testing micro channel with different concentration glucose solution including 10 wt %, 2 wt %, 1 wt %, 0.2 wt % and 0.01 wt %, respectively. The noise caused from graphene crystal orientation and contact resistance differences has the same influence on I_{DS} of both tested solution and DI water, and can be reduced and eliminated in differential output.

Table 2 List of Δ I_{DS} and Sensitivity towards different glucose concentration of differential output structure testing

Concen-tration	10%	2%	1%	0.2%	0.01%	DI
ΔI_{DS} /μA	27.28	22.04	19.81	12.99	10.39	10.37
S	33.6%	21.6%	17.9%	4.6%	1.1%	0%

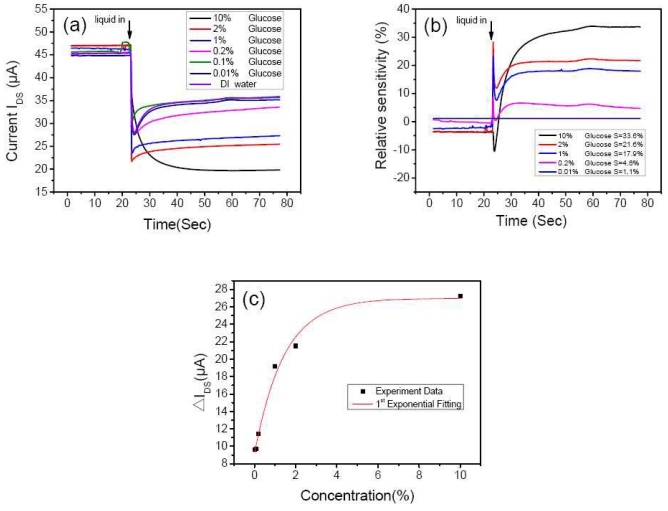

FIGURE 4 Source-to-drain current profile of differential structure of glucose solution. (a) I_{DS} versus time response under different concentration of glucose solution including 10 wt %, 2 wt %, 1 wt %, 0.2 wt %, 0.1 wt % and 0.01 wt %. (b) Relative sensitivity versus time response under different concentration of glucose solution. The relative sensitivity ranges from 33.6 % to nearly 1.1

Nanoscale Accepted Manuscript

This journal is © The Royal Society of Chemistry 2012

%. (c) the ΔI_{DS} versus Concentration curve shows the resolution in different concentration.

The fluctuation caused in experiment would affect graphene ribbons in both of testing and reference micro channel, and has been reduced even eliminated. Sensitivity increases exponentially with the increase of concentration of glucose as shown in Figure 4c, the highest resolution is 0.01 wt %. We can also find that the slope is higher in low concentration and ΔI_{DS} changed linearly in the range of 0.01 % to 0.1%. In the higher concentration, the device is saturated and could not distinguish the solution with different concentration.

We also prepare four kinds of concentration of normal saline including 0.09 wt %, 0.018 wt %, 0.009 wt % and 0.0009 wt %, respectively. The differential I_{DS} and relative sensitivity S ranges from 22.8 % in the concentration of 0.09 wt % to 0.86 % in the concentration of 0.0009 wt % are shown in Table 3. The highest saline resolution in differential structure is 0.0009 wt %. The glucose is non-electrolyte and could not ionize, which is different from saline solution measurement. As shown in Figure 4 (c) and Figure 5 (c), the ΔI_{DS} increases sharply in the range of 0.01 ~ 2 % (glucose) and 0.0009~0.018wt % (saline), respectively, and goes into saturation in higher concentration region, the reason for that is because our device with the size of micrometers. It means our device shows outstanding resolution property and can be used for ultra low concentration of analytes detection.

Table 3 List of ΔI_{DS} and Sensitivity towards different saline concentration of differential output structure testing

Concentration	0.09%	0.018%	0.009%	0.0009%	DI
ΔI_{DS} /μA	33.52	24.93	26.22	17.46	16.5
S	22.8%	18.9%	14.7%	0.86%	0%

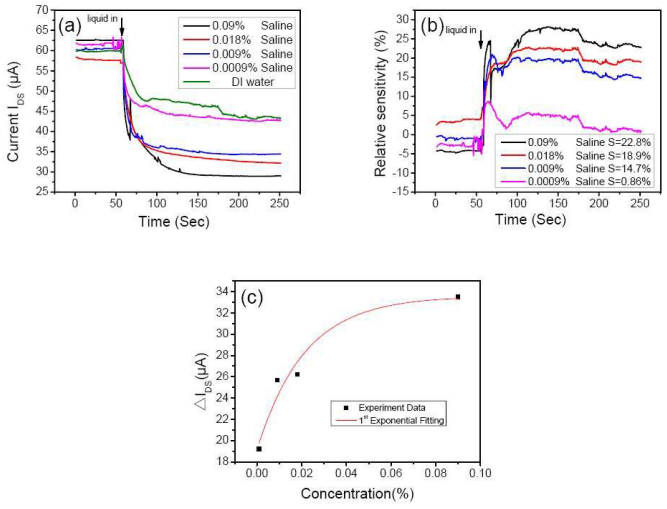

FIGURE 5 Source-to-drain current profile of differential structure of normal saline solution. (a) I_{DS} versus time response under different concentration of normal saline solution including 0.09 wt %, 0.018 wt %, 0.009 wt %, and 0.0009 wt %. (b) Relative sensitivity versus time response under different concentration of normal saline solution. The relative sensitivity ranges from 22.8 % to nearly 0.86 % . (c) the ΔI_{DS} versus Concentration curve shows the resolution in different concentration.

4. Conclusions

We have successfully fabricated 1×4 biosensor array with differential output based on monocrystal domain graphene ribbon. The fluctuation caused in crystal defect and experiment process has been reduced even eliminated by differential output structure. We have fabricated high quality monocrystal graphene domain which has millimeter size via chemical vapor deposition method. The source-to-drain current response time is shorter than 0.5 second. Dirac point shifts to negative voltage with increasing pH value because doping effect plays a dominant role in the changing of graphene ribbon conductivity. The highest resolution of glucose and normal saline are 0.01 wt % and 0.0009 wt %, respectively. Our device shows superior properties and has higher sensitivity and resolution in the lower concentration. If a lower concentration of virus molecules or cancer cells can be detected, cancer early detection technique will be improved significantly.

Acknowledgements

This work was financially supported by grants from the National Natural Science Foundation of China (No. 91123018, 61172040, 61172041), Shaanxi Natural Science Foundation (2014JM7277), and the Fundamental Research Funds for the Central Universities. The SEM work was done at International Center for Dielectric Research (ICDR), Xi'an Jiaotong University, Xi'an, China; The authors also thank Ms. Dai and Mr. Yang for their help in using SEM.

Conflict of interest

The authors declare that there is no conflict of interests regarding the publication of this article.

Notes and references

1 A. K Geim and K. S Novoselov, *Nat.Mater.*, 2007, **6**, 183-191.
2 A. K. Geim, *Science*, 2009, **324**, 1530-1534.
3 K. S. Novoselov, A. K. Geim, S. V. Morozov, D. Jiang, Y. Zhang, S. V. Dubonos, I. V. Grigorieva and A. A. Firsov, *Science*, 2004, **306**, 666-669.
4 Y. Cui, et al, *Science*, 2001, **293**, 1289-1292.
5 M. T. Martinez, et al, *Nano letters*, 2009, **9**, 530-536.
6 A. Kaniyoor, R. I. Jafri, T. Arockiadoss and S. Ramaprabhu, *Nanoscale*, 2009, **1**, 382-386.
7 S. Alwarappan, A.Erdem, C. Liu and C.-Z. Li, *J. Phys. Chem. C*, 2009, **113**, 12920-12924.
8 S. Alwarappan, A.Erdem, C. Liu and C.-Z. Li, *J. Phys. Chem. C*, 2009, **113**, 8853-8857.
9 Yasuhide Ohno, Kenzo Maehashi, and Kazuhiko Matsumoto, *J. AM. CHEM. SOC.*, 2010, **132**, 18012-18013.
10 Wangyang Fu, Cornelia Nef, Oren Knopfmacher, Alexey Tarasov, Markus Weiss et al., *Nano Lett.*, 2011, **11**, 3597-3600.
11 Ying Wang, Yeming Li, Longhua Tang, Jin Lu, Jinghong Li, *Electrochemistry Communications*, 2009, **11**, 889-892.

Nanoscale Accepted Manuscript

12 F. Schedin, A. K. Geim, S. V. Morozov, E. W. Hill, P. Blake, M. I. Katsnelson and K. S. Novoselov, *Nat. Mater.*, 2007, **6**, 652-655.
13 Y. M. Lin et al., *Nano Lett.*, 2008, **8**, 2119-2125
14 K. I. Bolotin, K.J. Sikes, Z. Jiang, M. Klima, G. Fudenberg, J. Hone, P. Kim, H.L. Stormer, *Solid State Comm.*, 2008, **146**, 351-355.
15 X. Du, I. Skachko, A. Barker, E. Y. Andrei, *Nat. Nanotechnol.* ,2008, **3**, 491-495.
16 Zengguang Cheng, Qiang Li, Zhongjun Li, Qiaoyu Zhou and Ying Fang, *Nano Lett.*, 2010, **10**, 1864-1868.
17 Fengnian Xia, Vasili Perebeinos, Yu-ming Lin, Yangqing Wu and Phaedon Avouris, *Nat. Nanotechnol.*, 2011, **6**, 179-184.
18 A. D. Franklin, A. A. Bol, W. Haensch, S. J. Han, *IEEE Electron Device Lett.*, 2011, **32**, 1035-1037.
19 L. Wang, I. Meric, P. Y. Huang, Y. Gao, H. Tran, T. Taniguchi, K. Watanabe, D. A. Muller, *Science*, 2013, **342**, 614-617.
20 Yuki Matsuda and Wei-Qiao Deng, *J. Phys. Chem. C*, 2010,**114**,17845-17850.
21 E. J. H. Lee, K. Balasubramanian, R. T. Weitz, M. Burghard, K. Kern, *Nat. Nanotechnol.,* 2008, **3**, 486–490.
22 Joshua T. Smith, Aaron D. Franklin, Damon B. Farmer and christos D. Dimitrakopoulos, *ACS NANO*, 2013, **7**, 3661-3667.
23 F. Xia, V. Perebeinos, Y. M. Lin, Y. Wu, P. Avouris, *Nat. Nanotechnol.*, 2011, **6**, 179-184.
24 W. C. Ren, L.B. Gao, L. P. Ma and H. M. Cheng, *New Carbon Mater.*, 2011, **26**, 71-80.
25 A. Reina, X. T. Jia, J. Ho, D. Nezich, H. B. Son, V. Bulovic, M. S. Dresselhaus and J.Kong, *Nano Lett.*, 2009, **9**, 30-35.
26 Quanfu Li, Weihua Liu, Tuo Qu, Juan Zhang, Xin Li, Qikun Wang and Xiaoli Wang, *RCS Adv.*, 2015, **5**, 2328-2332.
27 Wei Liu, Hong Li, Chuan Xu, Yasin Khatami, Kaustav Banerjee, *Carbon*, 2011, **49**, 4122-4130.
28 Sang-Min Kim, Jae-Hyun Kim, Kwang-Seop Kim, Yun Hwangbo, Jong-Hyuk Yoon, Eun-Kyu Lee, Jaechul Ryu, Hak-Joo Lee, Seungmin Cho and Seung-Mo Lee, *Nanoscale*, 2014, **6**, 4728-4734.
29 Xuesong Li, Carl W. Magnuson, Archana Venugopal, Jinho An, JiWon Suk, Boyang Han, Mark Borysiak, Weiwei Cai, Aruna Velamakanni, Yanwu Zhu, Lianfeng Fu, Eric M. Vogel, Edgar Voelkl, Luigi Colombo and Rodney S. Ruoff, *Nano Lett.*, 2010, **10**, 4328-4334.
30 Zheng Yan, Zhiwei Peng and James M. Tour, *Acc. Chem. Res.*, 2014, **47**, 1327-1337.
31 X. S. Li, W. W. Cai, J. H. An, S. Kim, J. Nah, D. X. Yang, R. Priner, A. Velamakanni, I. Jung, E. Tutuc, S. K. Banerjee, L. Colombo and R. S. Ruoff, *Science*, 2009, **324**, 1312-1314.
32 Yasuhide Ohno, Kenzo Maehashi, Yusuke Yamashiro and Kazuhiko Matsumoto, *Nano Lett.*, 2009, **9**, 3318-3322.

Nanoscale Accepted Manuscript

 This journal is © The Royal Society of Chemistry 2012